行政院國家科學委員會補助專題研究計畫 □ 成 果 報 告 ■期中進度報告

（零場積分方程及其工程應用（1/3））

計畫類別：■ 個別型計畫　　□ 整合型計畫
計畫編號：NSC 97－2221－E－019－015-MY3
執行期間：　2008 年 08 月 01 日至　2009 年 07 月 31 日

計畫主持人：陳正宗 終身特聘教授
共同主持人：
計畫參與人員： 李應德 先生

成果報告類型(依經費核定清單規定繳交)：■精簡報告　□完整報告

本成果報告包括以下應繳交之附件：
□赴國外出差或研習心得報告一份
□赴大陸地區出差或研習心得報告一份
□出席國際學術會議心得報告及發表之論文各一份
□國際合作研究計畫國外研究報告書一份

處理方式：除產學合作研究計畫、提升產業技術及人才培育研究計畫、列管計畫及下列情形者外，得立即公開查詢
□涉及專利或其他智慧財產權，□一年□二年後可公開查詢

執行單位：國立臺灣海洋大學 河海工程學系

中　華　民　國　98　年　06　月　07　日

Part I: Torsion problem (2008~2009)

A systematic method for a circular torsion problem with circular holes and/or inclusions

Abstract

In this project, a systematic approach is proposed to calculate the torsional rigidity and stress of a circular bar containing multiple circular inclusions. To fully capture the circular geometries, the kernel function is expanded to the degenerate form and the boundary density is expressed into Fourier series. The approach is seen as a semi-analytical manner since error purely attributes to the truncation of Fourier series. By collocating the null-field point exactly on the real boundary and matching the boundary condition, a linear algebraic system is obtained. Convergence study shows that only a few number of Fourier series terms can yield acceptable results. Finally, torsion problems are revisited to check the validity of our method. Not only the torsional rigidities but also the stresses of multiple inclusions are also obtained by using the present approach.

Keywords: torsional rigidity, null-field integral equation, degenerate kernel, Fourier series

本計畫中，我們提出一套系統性的方法來計算圓形桿含圓形置入物之扭轉剛度與應力。為了充分利用圓形幾何特性，我們將核函數展成退化核形式，而邊界未知密度函數則使用傅立業級數來展開。本法可視為一套半解析的方法，因為誤差僅來自於傅立業係數的擷取項多寡。我們將零場點準確的佈於問題的邊界上並滿足邊界條件後，可得一線性代數系統。收斂測試結果顯示我們只須取少數個傅立業級數的項數，就可到達令人滿意的結果。最後，幾個扭轉問題將被重新探討來驗證我們所提方法的正確性。含置入物的扭轉桿之扭轉剛度與應力將使用本法來求得。

關鍵字：扭轉剛度、零場積分方程、退化核函數、傅立業級數

1. Introduction

In the past, multiply-connected Laplace problems have been solved either by conformal mapping or by other techniques. Ling [10] solved the torsion problem of a circular bar with several holes. Muskhelishvili [13] solved the problem of a circular bar reinforced by an eccentric circular inclusion. Chen and Weng [6] have introduced conformal mapping with a Laurent series expansion to analyze the Saint-Venant

torsion problem. They concerned with an eccentric bar of different materials with an imperfect interface under torque. Since the conformal mapping is limited to the doubly-connected region, it encounters difficulty for multiple inclusions. Therefore, many researchers have paid more attentions on other techniques or numerical methods. Caulk [2] developed a special boundary integral method to deal with the problem of a torsion bar with circular holes. Katsikadelis and Sapountzakis [7] used the boundary element method to solve the problem of an elliptic bar including one and two elliptic inclusions. Also, a practical problem of a rectangular concrete containing a Steel-I beam was concerned in their research. Later, Sapountzakis and Mokos [16] extended to deal with the nonuniform torsion problem that the composite bar is subject to an arbitrarily concentrated or distributed twisting moment. Shams-Ahmadi and Chou [17] used the complex variable boundary element method (CVBEM) to solve the torsion problem of composite shafts with arbitrary number of inclusions of different materials. Petrov [15] developed an effective technique of boundary element method (BEM) to determine torsion, shear and other characteristics of beam cross-sections of arbitrary complex shape including multiply-connected cross sections. Tang [18] utilized the singular and hypersigular formulations to solve the torsion problem with inclusions and/or cracks.

Caulk [2] used the special BIEM to determine the torsional rigidity of a circular bar with circular holes, and he pointed out that Ling's result of three holes deviated from his data. Chen *et al*. [5] supported the Caulk's comment by using the null-field integral approach. On the other hand, Bird and Steele [1] found the discrepancy between the Naghdi's solution [14] and their data for the beam bending problem with four holes. Also, Chen *et al*.'s result [3] agreed with the Naghdi's result. Following the success of [5], we extend to solve torsion problems with multiple circular inclusions.

In this project, the null-field integral equation is utilized to solve the Saint-Venant torsion problem of a circular bar with circular inclusions. The mathematical tools, the degenerate kernel for the fundamental solution and Fourier series for the boundary density, are utilized in the null-field integral formulation. By collocating the null-field point exactly on the real boundary and matching the boundary condition, the linear algebraic system is obtained and the unknown Fourier coefficients can be easily determined. Then, series solutions for the warping function, torsional rigidity and stress are obtained. Convergence study is also addressed. Numerical examples were given to show the validity and efficiency of our formulation.

2. Formulation of the problem

A circular bar containing N circular inclusions bounded to the contours B_k ($k = 0,1,2,\cdots,N$) is shown in Fig. 1. We define

$$B = \bigcup_{k=0}^{N} B_k \ . \tag{1}$$

The radii of circular bar and inclusions are a_0 and a_i ($i = 1,2,\cdots,N$), respectively. The circular bar twisted by couples applied at the end is taken into consideration. Following the theory of Saint-Venant torsion [19], we assume the displacement to be

$$u = -\alpha yz\,,\quad v = \alpha xz\,,\quad w = \alpha\varphi(x,y)\,, \tag{2}$$

where α is the angle of twist per unit length along the z direction and φ is the warping function. Based on the relation of strain and displacement defined in the elasticity book [19], we have the strain components as follows:

$$\varepsilon_x = \varepsilon_y = \varepsilon_z = \gamma_{xy} = 0\,,\quad \gamma_{xz} = \alpha(\frac{\partial\varphi}{\partial x} - y)\,,\quad \gamma_{yz} = \alpha(\frac{\partial\varphi}{\partial y} + x)\,. \tag{3}$$

By applying the Hooke's law, the stress components are

$$\sigma_x = \sigma_y = \sigma_z = \sigma_{xy} = 0\,,\quad \sigma_{xz} = \mu\alpha(\frac{\partial\varphi}{\partial x} - y)\,,\quad \sigma_{yz} = \mu\alpha(\frac{\partial\varphi}{\partial y} + x)\,, \tag{4}$$

where μ is the shear modulus. There is no distortion in the planes of cross sections since $\varepsilon_x = \varepsilon_y = \varepsilon_z = \gamma_{xy} = 0$. By substituting Eq.(4) into the equilibrium equation [19], we have the warping function which satisfies the Laplace equation

$$\frac{\partial^2\varphi}{\partial x^2} + \frac{\partial^2\varphi}{\partial y^2} = 0 \quad \text{in } D, \tag{5}$$

where the body forces (F_x, F_y and F_z) are neglected and D is the domain of interest. On the cylinder surface, the stress states in Eq.(4) result in zero traction of $t_x = t_y = 0$. The only nonzero traction is t_z. Since there is no external traction, t_z, on the cylindrical surface, we have

$$t_z = \sigma_{xz}n_x + \sigma_{yz}n_y = \mu\alpha(\frac{\partial\varphi}{\partial x}n_x + \frac{\partial\varphi}{\partial y}n_y - yn_x + xn_y) = 0\,. \tag{6}$$

Therefore, the bracket in Eq.(6) is equal to zero and we have the boundary condition as follows:

$$\frac{\partial\varphi}{\partial x}n_x + \frac{\partial\varphi}{\partial y}n_y = \nabla\varphi\cdot\mathbf{n} = \frac{\partial\varphi}{\partial n} = yn_x - xn_y\,. \tag{7}$$

For the ideal boundary between the matrix and inclusions, the continuity condition for the displacement and equilibrium condition for traction on the interface [13] yield:

$$\varphi^M = \varphi^I \quad \text{on } B_i, \tag{8}$$

$$\mu_0 \frac{\partial \varphi_i^M}{\partial n} - \mu_i \frac{\partial \varphi_i^I}{\partial y} = (\mu_0 - \mu_i)(y n_x - x n_y) \quad \text{on } B_i, \tag{9}$$

where the superscripts "*I*" and "*M*" denote the inclusion and matrix, respectively, B_i is the *i*th interface boundary, μ_0 is the shear modulus for the matrix and μ_i is the shear modulus for the *i*th inclusion.

3. Method of solution

3.1 The conventional version

The integral equation for the domain point can be derived from the third Green's identity [6], we have

$$2\pi\varphi(x) = \int_B T(s,x)\varphi(s)\,dB(s) - \int_B U(s,x)\psi(s)\,dB(s), \quad x \in D, \tag{10}$$

$$2\pi \frac{\partial \varphi(x)}{\partial n_x} = \int_B M(s,x)\varphi(s)\,dB(s) - \int_B L(s,x)\psi(s)\,dB(s), \quad x \in D, \tag{11}$$

where *s* and *x* are the source and field points, respectively. By moving the field point to the boundary, Eqs.(10) and (11) reduce to

$$\pi\varphi(x) = C.P.V.\int_B T(s,x)\varphi(s)\,dB(s) - R.P.V.\int_B U(s,x)\psi(s)\,dB(s), \; x \in B, \tag{12}$$

$$\pi \frac{\partial \varphi(x)}{\partial n_x} = H.P.V.\int_B M(s,x)\varphi(s)\,dB(s) - C.P.V.\int_B L(s,x)\psi(s)\,dB(s), \; x \in B, \tag{13}$$

where *R.P.V.*, *C.P.V.* and *H.P.V.* denote the Riemann principal value, Cauchy principal value and Hadamard principal value, respectively. Once the field point *x* locates outside the domain ($x \in D^c$), we obtain the dual null-field integral equations as shown below

$$0 = \int_B T(s,x)\varphi(s)\,dB(s) - \int_B U(s,x)\psi(s)\,dB(s), \quad x \in D^c, \tag{14}$$

$$\pi \frac{\partial \varphi(x)}{\partial n_x} = H.P.V.\int_B M(s,x)\varphi(s)\,dB(s) - C.P.V.\int_B L(s,x)\psi(s)\,dB(s), \; x \in B, \tag{15}$$

where D^c is the complementary domain. Equations (11), (12), (14) and (15) are conventional formulations where the point can not be located on the real boundary. Singularity occurs and concept of principal values is required once Eqs.(12) and (13) are considered.

3.2 The present version

By introducing the degenerate kernels [5], the collocation point can be located on the real boundary free of facing singularity. Therefore, the representations of integral equations including the boundary point can be written as

$$2\pi\varphi(x) = \int_B T(s,x)\varphi(s)\,dB(s) - \int_B U(s,x)\psi(s)\,dB(s), \quad x \in D \cup B, \tag{16}$$

$$2\pi\frac{\partial\varphi(x)}{\partial n_x} = \int_B M(s,x)\varphi(s)\,dB(s) - \int_B L(s,x)\psi(s)\,dB(s), \quad x \in D \cup B, \tag{17}$$

and

$$0 = \int_B T(s,x)\varphi(s)dB(s) - \int_B U(s,x)\psi(s)dB(s), \quad x \in D^c \cup B, \tag{18}$$

$$0 = \int_B M(s,x)\varphi(s)dB(s) - \int_B L(s,x)\psi(s)dB(s), \quad x \in D^c \cup B, \tag{19}$$

once the kernels are expressed in term of an appropriate degenerate form. It is noted that x in Eqs.(16)-(19) can exactly be located on the real boundary.

For the boundary densities, we apply the Fourier series expansions to approximate the potential φ and its normal derivative ψ on the boundary

$$\varphi(s_k) = a_0^k + \sum_{n=1}^{\infty}(a_n^k \cos n\theta + b_n^k \sin n\theta), \quad s_k \in B_k, \quad k = 1,2,\cdots,N, \tag{20}$$

$$\psi(s_k) = p_0^k + \sum_{n=1}^{\infty}(p_n^k \cos n\theta + q_n^k \sin n\theta), \quad s_k \in B_k, \quad k = 1,2,\cdots,N, \tag{21}$$

where a_n^k, b_n^k, p_n^k and q_n^k are the Fourier coefficients.

It is worthy of noting that our approach can yield the same linear algebraic equation derived from boundary integral equation in Eqs.(12) and (13). However, the procedure is quite different although collocation points are located on the real boundary for both the conventional BIEM and the present approach. For the conventional BEM, it is necessary to calculate the singular or hypersingular integral by using the sense of principal value. Our approach is free of calculating principal value due to the introduction of the degenerate kernel since the kernel functions were separated into two parts, interior and exterior parts. If the appropriate kernels (interior and exterior parts) are chosen, we can easily obtain the same linear algebraic equation derived from the conventional BIE and free of calculating principal value. After obtaining the Fourier coefficients, the torsional rigidity can be easily determined as follows:

$$G = \mu\int_D (x^2 + y^2)\,dD - \mu\sum_{k=1}^{N}\int_{B_k} \varphi\frac{\partial\varphi}{\partial n}dB_k\,, \tag{22}$$

4. Illustrative examples and discussions

In this section, we revisit the torsion problems with inclusions and/or holes which have been solved by Muskhelishvili [13], Petrov [15], Tang [18], Ling [10], and Kuo and Conway [8, 9] for demonstrating the validity of present method.

Example 1: A circular bar with an eccentric inclusion

A circular bar of radius R_0 with an eccentric circular inclusion of radius R_1 is shown in Fig. 2. The ratio of R_1/R_0 and e_x/R_0 are 0.3 and 0.6, respectively. Fig. 3 shows the torsional rigidity versus the number of Fourier series term when μ_1/μ_0 is equal to 0.6. It is found that the solution converges fast by using only fourteen terms of Fourier series. The results of torsional rigidity for different values of μ_1/μ_0 are shown in Table 1. For verifying our results, the exact solution of Muskhelishvili and the result of integral formulation by Tang [18] are shown in Table 1 for comparison. The present results match very well with the exact solution derived by Muskhelishvil and are better than those of Tang [18]. For the rigid inclusion, the torsional rigidity becomes infinity as shown in Table 1.

The limiting case ($\mu_1 = 0$, e_x=0.5) is also used to check the present formulation. The exact solution of Muskhelishvili [13] is also calculated by using the exact formula. The results are shown in Table 2. It is found that the results of present method matches well with those of the Muskhelishvili's data [13] and are better than those of the Petrov's results [15]. However, the Lurje's solution [11] is smaller than those of the Petrov's, Muskhelishvili's and our results. Since three various methods obtain the consistent result, the formulae of Lurje [11] needs further check. The stresses along the inner and outer boundaries for $\lambda = 0.3$ and $p = 0.4$ [10] are shown in Table 3. It is found that the errors are less than two percents. The stresses on the x axis in domain are shown in Table 4. The results are very close to the Ling's analytical results obtained from the bipolar coordinate system.

Example 2: A circular rod with a ring of circular inclusions

In this example, we revisit the problems of a circular rod with a ring of circular inclusions investigated by Kuo and Conway [8] as shown in Fig. 4. Three cases are given in their article as

Case 1: $\frac{b}{a}=\frac{3}{4}$, $\frac{\lambda}{a}=\frac{1}{8}$, $\frac{\delta}{a}=\frac{1}{2}$, $\frac{G_2}{G_1}=30$, $k=8$,

Case 2: $\frac{b}{a}=\frac{3}{4}$, $\frac{\lambda}{a}=\frac{1}{8}$, $\frac{\delta}{a}=\frac{1}{2}$, $\frac{G_2}{G_1}=5$, $k=3$,

Case 3: $\frac{b}{a}=\frac{1}{2}$, $\frac{\lambda}{a}=\frac{1}{4}$, $\frac{\delta}{a}=0$, $\frac{G_2}{G_1}=29.4$, $k=4$.

The results of the present approach are shown in Table 5. It is found that the results of our approach are slightly different from the Kuo and Conway's results. For the Case 3, Kuo and Conway [8] claimed that they obtained the nondimensional torsional rigidity 1.57 analytically and 1.53 in the experiment. It seems that they obtained consistent results. However, the data of FE solution 1.77 obtained by Murakami &

Yamakawa [12] agrees well with the result of our approach. In this case, our result deviates from the experiment data of Kuo and Conway [8] but converges to the data of finer mesh using FEM by Murakami and Yamakawa [12]. In general, the numerical analysis is developed to predict the data before experiment. However, we always find that the results have differences between the numerical analysis and experiment data. We may wonder that the numerical result may not be correct if the two results deviate. As we know, the mathematical model is established under certain assumptions. Therefore, the mathematical model is always simpler than the real problem. If the mathematical model has the analytical or exact solution, it is the basic solution for comparison with the numerical result. For the real problem, many uncertain conditions exist in the experiment. Valid experimental data need special care. The inconsistency between the experimental data and numerical results stems from many reasons. So, the mathematical model is continuously modified by adding specific consideration.

Example 3: A circular rod with several rings of circular inclusions

In this example, we consider a circular rod with several rings of circular inclusions proposed by Kuo and Conway [9]. Four cases were addressed

Case 1: $\frac{b_1}{a}=\frac{3}{8}$, $\frac{b_2}{a}=\frac{3}{4}$, $\frac{\lambda}{a}=\frac{1}{8}$, $\frac{G}{G_0}=30$, $j=2$, $k=6$,

Case 2: $\frac{b_1}{a}=\frac{1}{4}$, $\frac{b_2}{a}=\frac{17}{32}$, $\frac{b_3}{a}=\frac{13}{16}$, $\frac{\lambda}{a}=\frac{3}{32}$, $\frac{G}{G_0}=30$, $j=3$, $k=6$,

Case 3: $\frac{b_1}{a}=\frac{3}{8}$, $\frac{b_2}{a}=\frac{3}{4}$, $\frac{\lambda}{a}=\frac{1}{8}$, $\frac{G}{G_0}=0$, $j=2$, $k=6$,

Case 4: $\frac{b_1}{a}=\frac{1}{4}$, $\frac{b_2}{a}=\frac{17}{32}$, $\frac{b_3}{a}=\frac{13}{16}$, $\frac{\lambda}{a}=\frac{3}{32}$, $\frac{G}{G_0}=0$, $j=3$, $k=6$.

The geometry sketch is shown in Fig. 5. The results of our approach and those of Kuo and Conway are shown in Table 6. In a similar situation of the previous example, the torsional rigidities deviate with those of Kuo and Conway's result. The reason may be explained in a similar way of Example 3.

5. Conclusions

Torsion problems with circular inclusions as well as holes have been successfully solved by using the present formulation. Our solutions match well with the exact solution if available and other solutions by using the integral formulation. Only 41 collocation points uniformly distributed on each boundary are required to obtain the accurate results of torsional rigidity with error less than 1 % after comparing with the exact solution. For the stress response, our approach also agrees

well with the analytical solution. The program was developed to deal with arbitrary number, different positions, various radii and shear moduli of inclusions. The proposed approach is free from calculating principal value, of boundary-layer effect, while the exponential convergence and the meshless method are included in the original elements and advantages of the method. Besides, the BIEs for the domain point or the null-field equation in our formulation can both be employed by exactly collocating the point on the real boundary thanks to the introduction of the degenerate kernels.

5. References

1. Bird MD, Steele CR (1991) Separated solution procedure for bending of circular plates with circular holes. J Appl Mech 59:398-404
2. Caulk DA (1983) Analysis of elastic torsion in a bar with circular holes by a special boundary integral method. J Appl Mech 50:101-108
3. Chen JT, Chen PY (2007) A semi-analytical approach for stress concentration of cantilever beams with holes under bending. J Mech 23(3):211-221
4. Chen JT, Hong H-K (1999) Review of dual boundary element methods with emphasis on hypersingular integrals and divergent series. Appl Mech Rev 52:17-33
5. Chen JT, Shen WC, Chen PY (2006) Analysis of circular torsion bar with circular holes using null-field approach. CMES 12:109-119
6. Chen T , Weng IS (2001) Torsion of a circular compound bar with imperfect interface. J Appl Mech 68:955-958
7. Katsikadelis JT, Sapountzakis EJ (1985) Torsion of composite bars by boundary element method. J Engng Mech 111:1197-1210
8. Kuo YM, Conway HD (1973) The torsion of composite tubes and cylinders. Int J Solids Struct 9:1553-1565
9. Kuo YM, Conway HD (1974) Torsion of cylinders with multiple reinforcement. J Eng Mech Div 100:221-233
10. Ling CB (1947) Torsion of a circular tube with longitudinal circular holes. Q Appl Math 5:168-181
11. Lurje AI (1970) Theory of elasticity. Nauka Publisher, Moscow (in Russian)
12. Murakami H, Yamakawa J (1998) Torsional wave propagation in reinforced concrete columns. Int J Solids Struct 35:2617-2637
13. Muskhelishvili NI (1963) Some basic problems of the mathematical theory of elasticity. P. Noordhoff, Groningen
14. Naghdi AK (1991) Bending of a perforated circular cylindrical cantilever. Int J Solids Struct 28(6): 739-749

15. Petrov EP (1997) Analysis of torsion and shear characteristics of beam cross-sections by the boundary element method. Int J BEM Commun 8:239-245
16. Sapountzakis EJ, Mokos VG (2001) Nonuniform torsion of composite bars by boundary element method. J Engng Mech, ASCE 127(9):945-953
17. Shams-Ahmadi M, Chou SI (1997) Complex variable boundary element method for torsion of composite shafts. Int J Numer Methods Engng 40:1165-1179
18. Tang RJ (1996) Torsion theory of the crack cylinder. Shanghai Jiao Tong University Publisher, Shanghai (in Chinese)
19. Timoshenko SP, Goodier JN (1970) Theory of Elasticity. McGraw-Hill, New York

Table1 Torsional rigidity of a circular bar with an eccentric inclusion

$\frac{\mu_1}{\mu_0}$	$2G/\pi\mu_0 R_0^4$		
	Muskhelishvili [13]	**Tang [18]**	**Present method (*M*=20)**
0	0.82370	0.82377	0.82370
0.2	0.89180	0.89181	0.89180
0.6	0.96246	0.96246	0.96246
1.0	1.00000	1.00000	1.00000
5.0	1.10800	1.10794	1.10800
20.0	1.25224	1.25181	1.25224
1000	9.19866	N/A	9.19866
10000	82.09883	N/A	82.09882
1000000	8101.10012	N/A	8101.09883

Table 2 Torsional rigidity of a circular bar with an eccentric hole

	$G/\mu_0 R_0^4$		
Present method	1.389 (34)	1.389 (66)	1.389 (130)
Petrov [15]	1.391 (32)	1.390 (64)	1.389 (130)
Lurje [11]	1.311		
Muskhelishvili [13]	1.389		

Note: the data in the parenthesis denotes number of degrees of freedom

Table 3 ξ_z **on the boundary for** λ**=0.3 and** p**=0.4**

ξ	$\eta=\alpha$			$\eta=\beta$		
	θ	$\frac{2}{\mu\tau D}\xi_z$ **[10]**	**Present method**	θ	$\frac{2}{\mu\tau D}\xi_z$ **[10]**	**Present method**
π	180°	1.166	1.166	180°	1.015	1.012
$\frac{3}{4}\pi$	154°18′	1.115	1.114	144°16′	0.881	0.881
$\frac{1}{2}\pi$	122°19′	1.011	1.011	104°12′	0.522	0.522
$\frac{1}{4}\pi$	73°55′	0.949	0.949	56°2′	0.068	0.067
0	0°	0.936	0.940	0°	-0.166	-0.167

Table 4 ξ_z **along the line of** $\xi=0$ **and** π **for** $\lambda=0.3$ **and** $p=0.4$

η	$\xi=\pi$			$\xi=0$		
	$\frac{x_1}{D}$	$\frac{2}{\mu\tau D}\xi_z$ **[10]**	**Present method**	$\frac{x_2}{D}$	$\frac{2}{\mu\tau D}\xi_z$ **[10]**	**Present method**
1.2384	0	1.166	1.166	0	0.940	0.940
1.4084	0.0446	1.097	1.096	0.1335	0.652	0.651
1.5784	0.0848	1.044	1.043	0.2342	0.420	0.418
1.7484	0.1208	1.009	1.010	0.3120	0.215	0.216
1.9784	0.1528	0.998	0.999	0.3730	0.026	0.026
2.0826	0.1800	1.015	1.012	0.4200	-0.166	-0.167

Table 5 Torsional rigidity of different cases for a circular ring with inclusions

Case	$\frac{b}{a}$	$\frac{\lambda}{a}$	$\frac{\delta}{a}$	$\frac{G_2}{G_1}$	k	$\frac{G_e}{G_1}$ **[8]**	$\frac{G_e}{G_1}$ **(Present)**
Case 1	$\frac{3}{4}$	$\frac{1}{8}$	$\frac{1}{2}$	30	8	1.2330	1.2924
Case 2	$\frac{3}{4}$	$\frac{1}{8}$	$\frac{1}{2}$	5	3	1.0466	1.0742
Case 3	$\frac{1}{2}$	$\frac{1}{4}$	0	29.4	4	1.5706	1 .7740

Table 6 Torsional rigidity of different cases for a circular bar with two and three rings of holes or inclusions

Case	$\frac{b_1}{a}$	$\frac{b_2}{a}$	$\frac{b_3}{a}$	$\frac{\lambda}{a}$	$\frac{G}{G_0}$	j	k	$\frac{G_{eff}}{G_0}$ **[9]**	$\frac{G_{eff}}{G_0}$ **(Present)**
1	$\frac{3}{8}$	$\frac{3}{4}$	--	$\frac{1}{8}$	30	2	6	1.1205	1.3553
2	$\frac{1}{4}$	$\frac{17}{32}$	$\frac{13}{16}$	$\frac{3}{32}$	30	3	6	1.0618	1.2332
3	$\frac{3}{8}$	$\frac{3}{4}$	--	$\frac{1}{8}$	0	2	6	0.9636	0.7493
4	$\frac{1}{4}$	$\frac{17}{32}$	$\frac{13}{16}$	$\frac{3}{32}$	0	3	6	0.9745	0.7800

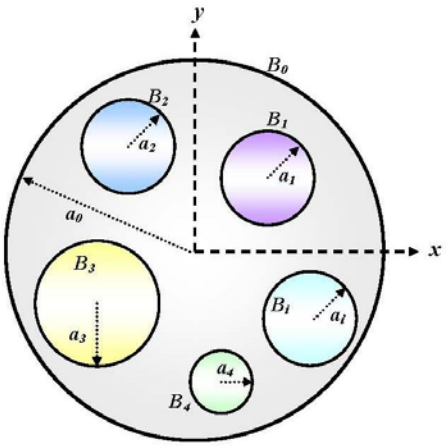

Fig. 1 Sketch of a circular bar with circular holes and/or inclusions under torsion

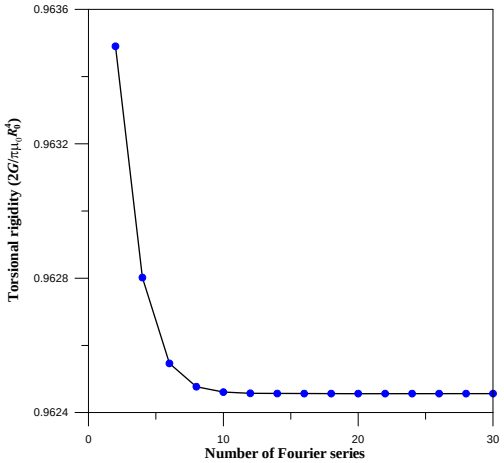

Fig. 3 Torsional rigidity versus number of truncated terms of Fourier series

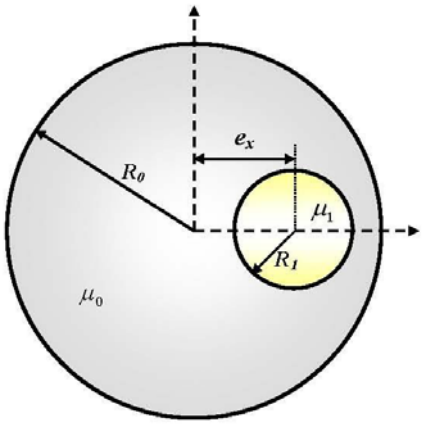

Fig. 2 Sketch of an eccentric circular inclusion problem

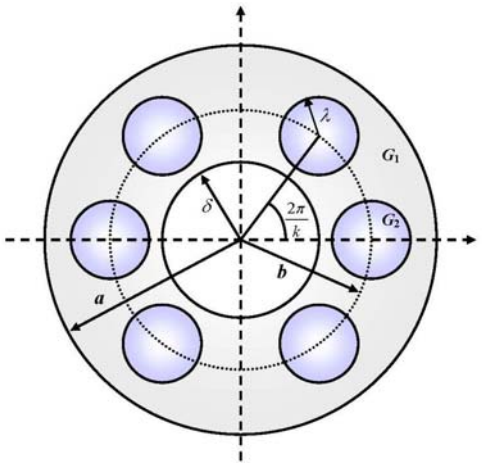

Fig. 4 A circular rod with a ring of circular inclusions

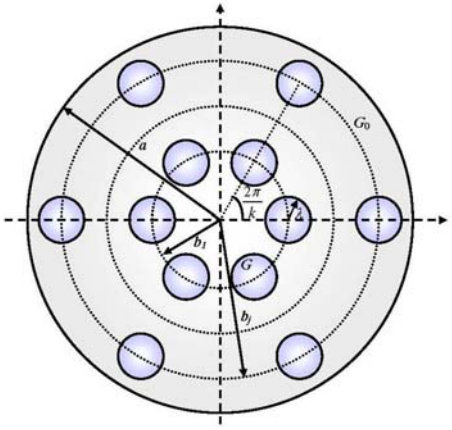

Fig. 5 A circular rod with several rings of circular inclusions

6. Self-evaluation

1. According to our proposal, we have succeeded in employing the null-field formulation to solve torsion problems with circular inclusions and/or holes in the first year.
2. SCI papers appear as shown below:

   J. T. Chen, W. C. Shen and P. Y. Chen, Analysis of circular torsion bar with circular holes using null-field approach, *Computer Modeling in Engineering and Sciences*, Vol.12, pp.109-119, 2006.

   J. T. Chen and Y. T. Lee, Torsional rigidity of a circular bar with multiple circular inclusions using the null-field integral approach, *Computational Mechanics*, Vol.44, No.2, pp.221-232, 2009.
3. For more details, please visit our web site of http://ind.ntou.edu.tw/~msvlab.